

**CRITICAL POINT OF
THE HONEYCOMB ANTIFERROMAGNETIC ISING MODEL
IN A NONZERO MAGNETIC FIELD: FINITE-SIZE ANALYSIS**

H. W. J. BLÖTE

Laboratorium voor Technische Natuurkunde, Postbus 5046, 2600 GA Delft, The Netherlands

F. Y. WU and X. N. WU

Department of Physics, Northeastern University, Boston, MA 02115, USA

Received 28 November 1989

In this paper we present highly accurate numerical results of the determination of the critical point of the antiferromagnetic Ising model in a nonzero magnetic field for the honeycomb lattice, including the critical fugacity of a nearest-neighbor exclusion lattice gas. We compute the correlation length of the Ising model using a transfer matrix approach, and locate the critical point from the data on the correlation lengths using finite-size analysis. For the purpose of a maximum numerical accuracy, the analysis is carried out by taking transfer matrices proceeding in two perpendicular directions of the lattice.

1. Introduction

In a recent letter¹ we have considered the antiferromagnetic Ising model on the honeycomb lattice in a nonzero magnetic field, and obtained a closed-form expression for its critical frontier, the line of critical points where the per-site partition function becomes nonanalytic. The system is described by the reduced Hamiltonian

$$-\beta\mathcal{H} = K \sum \sigma_i \sigma_j + L \sum \sigma_i \quad (1)$$

where the first summation is over all interacting pairs and the second summation is over all lattice sites. The per-site partition function in the thermodynamic limit is

$$\kappa(K, L) = \lim_{N \rightarrow \infty} [Z(K, L)]^{1/N}, \quad (2)$$

where

$$Z(K, L) = \sum_{\sigma_i = \pm 1} e^{-\beta\mathcal{H}} \quad (3)$$

is the partition function, and N is the total number of Ising spins.

Our analysis was based on a consideration of an invariance property of the critical frontier in an enlarged parameter space, a consideration which has led to a closed-form expression of the critical frontier containing several undetermined constants. A major step

of our analysis was, then, the determination of these constants using highly accurate numerical results of a finite-size analysis,² the detail of which was, however, not given in Ref. 1 due to the limitation of space. In this paper we present the details of this finite-size analysis.

As a convenient tool for carrying out the finite-size analysis, we have chosen the phenomenological renormalization of the correlation length,³ a method which has been demonstrated to yield accurate results for the same problem on the square lattice.⁴ In this approach, we use a transfer matrix technique to determine correlation lengths numerically for lattices of size $n \times \infty$ for a number of values of the finite-size parameter n , and with periodic boundary conditions in the finite direction. The data for different values of n are analyzed systematically to extract the best values for the critical point of the bulk system.

The organization of the paper is as follows. In Sec. 2 we formulate the transfer matrix technique, and in Sec. 3 we describe the finite-size analysis. Specific details for analyzing the honeycomb lattice are presented in Sec. 4, and numerical results are given in Sec. 5.

2. The Transfer Matrix

In this section we formulate the transfer-matrix method in a way used by Lieb *et al.*⁵ Since this is not the usual definition, a self-contained formulation is given for the reader's convenience.

Consider a strip of a lattice consisting of l rows of n spins. Two spins may interact only if they lie in the same row or in neighbouring rows. Denote the j th spin in the i th row by s_{ij} and introduce the notation $\mathbf{s}_i \equiv \{s_{i1}, s_{i2}, \dots, s_{in}\}$. Then, the Hamiltonian of the strip can be written as

$$\mathcal{H}_l = \sum_{i=1}^l h_i(\mathbf{s}_i, \mathbf{s}_{i-1}). \quad (4)$$

Here, an index i has been appended to the row Hamiltonian h to allow the possibility that the interactions may be row-dependent. Next, a restricted partition sum is defined as

$$Z^{(i)}(\mathbf{s}_i) = \sum_{\mathbf{s}_1, \mathbf{s}_2, \dots, \mathbf{s}_{i-1}} \exp(-\beta \mathcal{H}_i). \quad (5)$$

Using (4), (5) can be rewritten as

$$Z^{(i)}(\mathbf{s}_i) = \sum_{\mathbf{s}_{i-1}} T_i(\mathbf{s}_i, \mathbf{s}_{i-1}) Z^{(i-1)}(\mathbf{s}_{i-1}) \quad (6)$$

where

$$T_i(\mathbf{s}_i, \mathbf{s}_{i-1}) = \exp[-\beta h_i(\mathbf{s}_i, \mathbf{s}_{i-1})] \quad (7)$$

are elements of a row-to-row transfer matrix \mathbf{T}_i . Thus, in matrix notation, we have

$$\mathbf{Z}^{(i)} = \mathbf{T}_i \mathbf{Z}^{(i-1)} = \mathbf{T}_i \mathbf{T}_{i-1} \dots \mathbf{T}_1 \mathbf{Z}^{(0)} \quad (8)$$

where $\mathbf{Z}^{(i)}$ is a column matrix. We will be primarily interested in the limit of $i \rightarrow \infty$, so that the situation at the ‘‘beginning’’ of the strip, described by the initial weights $\mathbf{Z}^{(0)}$, is unimportant.

Suppose that the lattice is periodic in the length direction (the direction perpendicular to the rows) with a periodicity p , i.e., $h_i = h_{i+p}$. Then, defining the complete transfer matrix as

$$\mathbf{T} = \mathbf{T}_p \mathbf{T}_{p-1} \dots \mathbf{T}_1, \quad (9)$$

we have

$$\mathbf{Z}^{(lp)} = \mathbf{T}^l \mathbf{Z}^{(0)}. \quad (10)$$

The expansion of $\mathbf{Z}^{(0)}$ in eigenvectors of \mathbf{T} then leads to

$$\begin{aligned} \mathbf{Z}^{(lp)} &= \sum_i c_i \lambda_i^l \\ &= c_1 \lambda_1^l [1 + (c_2/c_1)(\lambda_2/\lambda_1)^l + \dots], \end{aligned} \quad (11)$$

where the c_i 's are constants, and λ_i is the i th eigenvalue of \mathbf{T} , arranged in decreasing order of magnitudes. For n finite, the two largest eigenvalues are nondegenerate, and we have the explicit dependence $\lambda_i = \lambda_i(t, n)$, where t is a ‘‘temperature-like’’ parameter. Our goal is to determine the value t_c at which the per-site free energy is nonanalytic.

We shall assume that the nonanalyticity of the free energy is accompanied with the onset of long-range order in the spin system. If long-range order exists, then λ_1 and λ_2 are asymptotically degenerate in the bulk, permitting the identification of the correlation length (in the length direction of the strip) as

$$\xi(t, n) = 1/\zeta \ln(\lambda_1/\lambda_2), \quad (12)$$

which diverges as $n \rightarrow \infty$. Here, ζ is a geometric factor such that ζn is the ratio between the actual *physical* width of a row of n spins and the actual *physical* length of a period (in the length direction) of a geometrically isotropic honeycomb lattice.⁶ The correlation length can now be calculated by means of numerical diagonalization of the transfer matrix for a range of values of n .

More generally, there are different correlation lengths ξ_i , each associated with an eigenvalue λ_i and pertaining to different correlation functions. From exact solutions we know that the correlation length (12) is associated with the spin-spin correlation. On the basis of renormalization group arguments⁷ which generalize exact solutions and, more generally, on conformal invariance,⁸ the asymptotic finite-size scaling behavior of the

correlation length at the critical point $t = t_c$ is found to be

$$\lim_{n \rightarrow \infty} \xi(t_c, n)/n = (2\pi x_H)^{-1}, \quad (13)$$

where x_H is the magnetic scaling dimension of the Ising model. (For the Ising model in two dimensions, the case we are considering, we have $x_H = \eta/2 = 1/8$.) Equations (12) and (13) form the basis of the finite-size analysis which we formulate in the next section.

3. Finite-Size Analysis

In this section we formulate the finite-size analysis using (12) and (13). Combining these two expressions, we write, for n finite,

$$n\zeta \ln[\lambda_1(t, n)/\lambda_2(t, n)] = 2\pi x_H, \quad x_H = 1/8. \quad (14)$$

The numerical procedure is then, for n fixed, to solve (14) for t as an estimate of the critical point t_c . Finite-size scaling^{2,9} then predicts that, as n increases, the solution of (14) converges to the critical point t_c . In practice, however, this convergence holds even if x_H is assigned an incorrect value, but this will result in a slower convergence ($\sim 1/n$). Consequently, a convergence appreciably faster than $1/n$ is an indication that the correct value of x_H has been used.

At criticality, corrections to the leading scaling behavior are expected to be algebraic. Denoting the solution of (14) as $t_{1,n}$, we therefore expect

$$t_{1,n} \approx t_c + an^{-b}. \quad (15)$$

Further iterated estimates $t_{2,n}$ (of t_c) are obtained by requiring, for n fixed,

$$t_{1,m} = t_{2,n} + a_n m^{-b_n}, \quad m = n, n+1, n+2, \quad (16)$$

(or $m = n, n+2$ and $n+4$ if n is restricted to even values) and solving for the three unknowns on the right-hand side of (16).

For the square Ising model in the absence of a field, we know that $b = 3$.¹⁰ Thus, alternatively, one can set $b_n = 3$ in (16) and use only two consecutive values of m . (The use of two values of m would also work even if $b \neq 3$, although the rate of convergence would be affected.)

The process can be further iterated, yielding $t_{3,n}$, etc. These iterations, however, tend to increase the numerical errors due to the truncation of decimal places in the calculation of the eigenvalues. The iteration process is stopped when these numerical errors grow too large, or when the series of estimates becomes too short so that its apparent convergence can no longer be judged.

It should also be mentioned that the critical point can also be determined without the explicit use of the value of x_H , by solving for t from

$$\xi(t, n)/\xi(t, m) = n/m. \tag{17}$$

While this method works well,⁴ it is slightly more sensitive to rounding errors associated with the (finite) numerical precision of computer calculations.

4. Application to the Honeycomb Lattice

In this section we present specific details of the application of the finite-size analysis to the Ising model on the honeycomb lattice. As an independent check of the accuracy of our numerical results, we have carried out two independent finite-size analyses using transfer matrices taken in two perpendicular lattice directions.

4.1. Transferring in a direction perpendicular to a lattice edge

We first apply the transfer matrix proceeding in a direction perpendicular to one set of lattice edges. A portion of the lattice, shown in Fig. 1, consists of three rows of n spins, denoted by s_1, s_2 and s_3 . It is readily seen that the periodicity of the lattice prescribes $p = 2$ and the geometric factor $\zeta = \sqrt{3}/2$.⁶

We adopt the rule that, whenever a new row of spins is appended to the lattice, only one-half of the interactions in which only new spins participate is accounted for in the associated single-row transfer matrix. Then, for the same reason, one-half of the interactions in which only old spins participate is also incorporated in the single-row transfer matrix. Thus, we have

$$\mathbf{T} = \mathbf{T}_2\mathbf{T}_1 \tag{18}$$

where

$$\mathbf{T}_i = \mathbf{T}_{h,3-i}^{1/2}\mathbf{T}_v\mathbf{T}_{h,i}^{1/2}, \quad i = 1, 2. \tag{19}$$

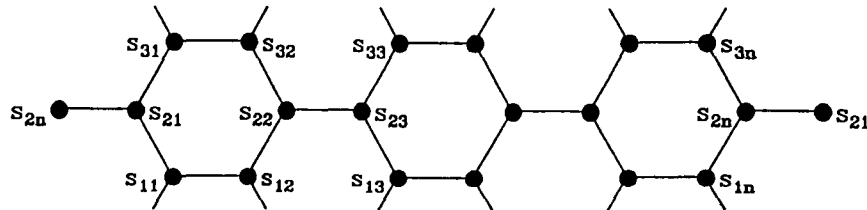


Fig. 1. Arrangement of the honeycomb lattice wrapped around a cylinder with the transfer matrix proceeding vertically perpendicular to one set of lattice edges.

Here, the diagonal matrices $\mathbf{T}_{h,i}$ account for the interactions within a row, and \mathbf{T}_v the interactions between neighbouring rows. Explicitly, they possess elements

$$T_{h,i}(\mathbf{s}, \mathbf{s}') = \prod_{j=i,i+2,\dots}^{n+i-2} \{\exp[Ks_j s_{j+1} + L(s_j + s_{j+1})] \delta_{s_j s'_j} \delta_{s_{j+1} s'_{j+1}}\} \quad (20)$$

$$T_v(\mathbf{s}, \mathbf{s}') = \prod_{j=1}^n \exp[Ks_j s'_j]$$

where, for simplicity, we have omitted the row indices. The cylindrical geometry imposes that n is even and $s_{n+1} = s_1$. The matrix \mathbf{T}_v can be trivially decomposed into commuting sparse matrices:

$$\mathbf{T}_v = \prod_{j=1}^n \mathbf{T}_{v,j} \quad (21)$$

with

$$T_{v,j}(\mathbf{s}, \mathbf{s}') = \exp[Ks_j s'_j] \prod_{i \neq j} \delta_{s_i s'_i} \quad (22)$$

This sparse-matrix decomposition not only leads to a large reduction of fast memory requirements, it also speeds up the calculation (since the number of scalar multiplications is greatly reduced). A further simplification follows by writing

$$\mathbf{T}_{v,j} = \mathbf{S}^{1-j} \mathbf{T}_{v,1} \mathbf{S}^{j-1}, \quad (23)$$

$$\mathbf{T}_v = [\mathbf{S} \mathbf{T}_{v,1}]^n,$$

where \mathbf{S} is the matrix representation of a translation operator which cyclically moves spin i to site $i - 1$. Thus only one sparse matrix multiplication algorithm needs to be explicitly programmed.

In the case of the nearest-neighbor exclusion lattice gas, we take $L \rightarrow \infty$, $K \rightarrow -\infty$, while keeping $z = e^{-2L-6K}$ fixed, where z is the fugacity of the lattice gas.¹¹ This corresponds to use, in place of (20),

$$T_{h,i}(\mathbf{s}, \mathbf{s}') = \prod_{j=i,i+2,\dots}^{n+i-2} z^{1-(s_j+s_{j+1})/2} \delta_{s_j s'_j} \delta_{s_{j+1} s'_{j+1}} f(s_j, s_{j+1}) \quad (24)$$

$$T_v(\mathbf{s}, \mathbf{s}') = \prod_{j=1}^n f(s_j, s'_j)$$

where

$$f(s_i, s_j) = \begin{cases} 0, & \text{if } s_i = s_j = -1 \\ 1, & \text{otherwise} \end{cases} \quad (25)$$

obtained by identifying $s_i = 1$ as representing the i th lattice site being empty.

Since the matrix (18) is symmetric, we can make use of the conjugate-gradient algorithm¹² to determine the largest eigenvalue. Under this scheme, the Perron-Frobenius theorem guarantees that the algorithm will converge to λ_1 , if all elements of the initial vector are chosen to be positive. The next largest eigenvalue λ_2 is obtained by application of the conjugate gradient algorithm to an initial vector with the correct symmetry, namely, an eigenvector antisymmetric with respect to the spatial inversion $s_i \leftrightarrow s_{n+1-i}$. This symmetry is obviously conserved by the transfer matrix.

4.2. Transferring in a direction parallel to a lattice edge

We next apply the transfer matrix proceeding in a direction parallel to one set of lattice edges. A portion of the lattice, shown in Fig. 2, consists of six rows of spins s_{ij} , $1 \leq i \leq 6$, $1 \leq j \leq n$. In this case we have $p = 3$ and $\zeta = 1/\sqrt{3}$. Along similar lines we define the transfer matrix

$$\mathbf{T} = \mathbf{T}_v^{1/2} \mathbf{T}_{h+} \mathbf{T}_v \mathbf{T}_{h-} \mathbf{T}_v^{1/2} \quad (26)$$

where

$$T_v(s, s') = \prod_{i=1}^n \exp(-Ks_i s'_i), \quad (27)$$

$$T_{h\pm}(s, s') = \prod_{i=1}^n \exp[Ks'_i(s_i + s_{i\pm 1}) \pm L(s_i + s'_i)].$$

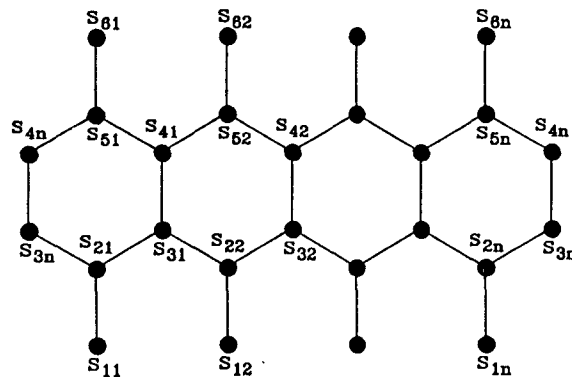


Fig. 2. Arrangement of the honeycomb lattice wrapped around a cylinder with the transfer matrix proceeding vertically parallel to one set of lattice edges.

Here, these expressions are obtained by applying a spin inversion redefinition to half of the horizontal rows, i.e., s_{ij} , $i = 2, 3, 6$ in Fig. 2, such that all vertical bonds become ferromagnetic and the magnetic field L acting on the inverted spins becomes $-L$. Note that \mathbf{T} is now symmetric when $L = 0$. In practice, since \mathbf{T}_v decomposes into n sparse, commuting, matrices, the determination of $\mathbf{T}_v^{1/2}$ is very simple, and the spin inversion redefinition guarantees that the elements of $\mathbf{T}_v^{1/2}$ are real for $K < 0$. Alternately, by introducing a decorating spin to an edge, we can use the explicit representation

$$\mathbf{T}_v^{1/2}(-K) = [e^{K/2}/\sqrt{2}]^n \mathbf{T}_v(K^*) \quad (28)$$

where $\tanh^2 K^* = -\tanh K > 0$.

The matrices \mathbf{T}_{h+} and \mathbf{T}_{h-} can also be decomposed into n sparse matrices:

$$\mathbf{T}_{h-} = \mathbf{T}_{h-,n} \dots \mathbf{T}_{h-,2} \mathbf{T}_{h-,1} \quad (29)$$

where

$$T_{h-,1}(\mathbf{s}, \mathbf{s}') = \exp[Ks_1(s'_1 + s'_2) - L(s_1 + s'_1)] \delta_{s'_1, s_{n+1}} \prod_{i=2}^n \delta_{s_i, s'_i}, \quad (30a)$$

$$T_{h-,i}(\mathbf{s}, \mathbf{s}') = \exp[Ks_i(s'_i + s'_{i+1}) - L(s_i + s'_i)] \prod_{j=1}^{i-1} \delta_{s_j, s'_j} \prod_{j=i+1}^{n+1} \delta_{s_j, s'_j} \quad (30b)$$

for $i = 2, 3, \dots, n-1$, and

$$T_{h-,n}(\mathbf{s}, \mathbf{s}') = \exp[Ks_n(s'_2 + s'_{n+1}) - L(s_n + s'_n)] \prod_{j=1}^{n-1} \delta_{s_j, s'_j}. \quad (30c)$$

Here, $\mathbf{s}' = (s_{21}, s_{22}, \dots, s_{2n})$ and $\mathbf{s} = (s_{31}, s_{22}, \dots, s_{2n}, s_{21})$ in (30a);

$$\mathbf{s}' = (s_{31}, s_{32}, \dots, s_{3,i-1}, s_{2i}, s_{2,i+1}, \dots, s_{2n}, s_{21})$$

and $\mathbf{s} = (s_{31}, s_{32}, \dots, s_{3i}, s_{2,i+1}, s_{2,i+2}, \dots, s_{2n}, s_{21})$ in (30b); and $\mathbf{s}' = (s_{31}, s_{32}, \dots, s_{3,n-1}, s_{2n}, s_{21})$ and $\mathbf{s} = (s_{31}, s_{32}, \dots, s_{3n})$ in (30c). Note that the action of $\mathbf{T}_{h-,i}$ can be represented by appending the spin s_{3i} in Fig. 2 to the lattice. Thus, since the last row is incomplete, matrices $\mathbf{T}_{h-,1}$ and $\mathbf{T}_{h-,n}$ are rectangular. The matrices $\mathbf{T}_{h-,2}, \dots, \mathbf{T}_{h-,n-1}$ can be brought into the same form by means of a translation operator just as in the case of $\mathbf{T}_{v,j}$ described above. The sparse matrix decomposition of \mathbf{T}_{h+} can be formulated similarly.

In the case of the nearest-neighbour exclusion lattice gas, we replace (27) by

$$T_v(\mathbf{s}, \mathbf{s}') = \prod_{i=1}^n f(\pm s_i, \mp s'_i) \quad (31)$$

$$T_{h\pm}(\mathbf{s}, \mathbf{s}') = \prod_{i=1}^n z^{1 \mp (s_i + s'_i)/2} f(\pm s_i, \pm s'_i) f(\pm s_{i\pm 1}, \pm s'_i),$$

where $f(s, s')$ has been defined in (25). The upper signs in the first line of (31) apply when the row number of s is a multiple of 4, and the lower signs apply otherwise. This alternation arises because we have shifted factors in (26) in order to keep all matrix elements finite. •

Since \mathbf{T} is not symmetric for $L \neq 0$, the usual methods of determining the largest eigenvalue do not work. We have adopted a method based on a direct iteration, i.e., the analysis of the sequence

$$\mathbf{u}^{(m)} = \mathbf{T}^m \mathbf{u}^{(0)}, \quad (m = 0, 1, 2, \dots), \quad (32)$$

which, in general, converges to the leading right-hand eigenvector of \mathbf{T} . When the analysis of $\mathbf{u}^{(m)}$ allowed an accurate estimate λ_s of a subdominant eigenvalue, the contribution of the corresponding eigenvector to $\mathbf{u}^{(m)}$ was suppressed by a multiplication of $\mathbf{T} - \lambda_s \mathbf{I}$. Furthermore, we have used the symmetry property that the transportation of \mathbf{T} is equivalent with a spin inversion. Let \mathbf{I} represent the spin inversion operation, i.e. operation, i.e.

$$I(s, s') = \prod_{i=1}^n \delta_{s_i, -s'_i}. \quad (33)$$

Then, it follows from the definition (27) that

$$\tilde{\mathbf{T}}_{h\pm} = \mathbf{I} \mathbf{T}_{h\mp} \mathbf{I}. \quad (34)$$

Since $\tilde{\mathbf{T}}$, is invariant under spin inversion, we have, from (26),

$$\tilde{\mathbf{T}} = \mathbf{I} \mathbf{T} \mathbf{I}, \quad (35)$$

so that the right- and left-hand eigenvectors \mathbf{R} and \mathbf{L} of \mathbf{T} are related by

$$\mathbf{L} = \mathbf{R} \mathbf{I}. \quad (36)$$

After a number of iteration steps, $\mathbf{u}^{(m)}$ is equal to the leading eigenvector up to a contribution of order ϵ , and the largest eigenvalue is equal to

$$(\mathbf{u}^{(m)} \mathbf{I} \mathbf{T} \mathbf{u}^{(m)}) / (\mathbf{u}^{(m)} \mathbf{I} \mathbf{u}^{(m)}) \quad (37)$$

up to a contribution of order ϵ^2 . Other methods, such as the hybrid iteration Hessenberg method,¹³ would produce contributions of order ϵ , which will slow down the rate of convergence as well as negatively affect the numerical accuracy. The second largest eigenvalue of \mathbf{T} was found similarly after orthogonalizing the initial vector with respect to the leading left-hand eigenvector. Particularly, we use in (32) the following initial vector

$$\mathbf{v}^{(0)} = \mathbf{u}^{(0)} - (\mathbf{u}_1 \mathbf{I} \mathbf{u}^{(0)}) \mathbf{u}_1 / (\mathbf{u}_1 \mathbf{I} \mathbf{u}_1), \quad (38)$$

where \mathbf{u}_1 is the eigenvector corresponding to λ_1 as found above,

5. Numerical Results

In this section we present numerical results obtained by applying the formulation of the previous sections to the honeycomb Ising model.

5.1. Transferring in a direction perpendicular to a lattice edge

In this case we have been able to solve (14) for even system sizes up to $n \leq 20$ (systems with odd n do not fit on a cylinder in this geometry). The solution was obtained i) by assigning a fixed value to L and solving for K (as t_c); ii) by assigning a fixed value to K and solving for L ; and, in the case of the lattice gas with nearest-neighbor exclusion interactions, iii) solving (14) for the fugacity z using the modified transfer matrices (24) (or (31) for transferring parallel to a lattice edge).

These numerical solutions usually allow iterated fits up to $t_{4,n}$. These latter data show a rapid apparent convergence, and serve as a basis for the best estimates which are shown as $t_c(1)$ in Table 1. These data are consistent with the assumption that in general the deviation $t_c - t_{4,n}$ are at most of the same order of magnitude as the differences $t_{4,n} - t_{4,n-1}$. This enables us to estimate the numerical accuracy. The estimated uncertainties in the last decimal places are given in parentheses.

Table 1. Best estimates of points on the critical frontier of the antiferromagnetic Ising model on the honeycomb lattice in the (K, L) plane. The first column specifies the line along which the critical point was located; the second column shows the temperature-like variable chosen for determining the critical point. The third column gives the best estimates $t_c(1)$ on the basis of the results obtained in Secs. 4.1 and 5.1, and the last column the best estimates $t_c(2)$ on the basis of results of Secs. 4.2 and 5.2. Estimated inaccuracies in the last decimal places are shown between parentheses.

line	t	$t_c(1)$	$t_c(2)$
$L = 0.0$	K	-0.65847895 (1)	-0.658478948 (1)
$L = 1.0$	K	-0.77371214 (2)	-0.773712145 (2)
$L = 2.0$	K	-1.03663932 (2)	-1.036639308 (3)
$L = 3.0$	K	-1.35050861 (2)	-1.350508591 (4)
$L = 4.0$	K	-1.67865230 (2)	-1.678652280 (4)
$L = 5.0$	K	-2.01061366 (2)	-2.010613643 (4)
$L \rightarrow \infty$	z	7.8517226 (8)	7.8517218 (2)
$K = -0.7$	L	0.58243137 (10)	0.582431408 (5)
$K = -0.8$	L	1.11988421 (10)	1.119884213 (5)
$K = -0.9$	L	1.52060436 (10)	1.520604370 (7)
$K = -1.0$	L	1.87599042 (10)	1.875990455 (10)
$K = -1.2$	L	2.53015420 (10)	2.530154228 (10)
$K = -1.5$	L	3.45812975 (10)	3.458129780 (10)
$K^{-1} = -1.5$	L		0.255031779 (5)
$K^{-1} = -1.3$	L		0.978598601 (5)
$K^{-1} = -1.1$	L		1.554262531 (7)
$K^{-1} = -0.9$	L		2.245417515 (10)
$K^{-1} = -0.7$	L		3.239969156 (10)

5.2. Transferring in a direction parallel to a lattice edge

In this case (14) was solved for system sizes up to $n = 19$. The results were subjected to extrapolation procedures as described above. The best estimates, obtained from $t_{4,n}$, are shown as $t_c(2)$ in Table 1. Comparing these results with $t_c(1)$, it appears that the apparent accuracy of $t_c(2)$ is better, even though the maximum system size of $n = 19$ is slightly smaller. However, we emphasize that the estimation of these errors is somewhat subjective. The method of estimation is the same for the results shown for both methods; the fact that the differences between these data agree with the errors quoted for $t_c(1)$ confirms that the estimated errors have the correct order of magnitude. Moreover, application of the same methods to shorter series $t_{1,n}$ leads to error bounds consistent to those in Table 1.

6. Acknowledgments

This research is supported in part by the National Science Foundation Grant No. DMR-8702596 and the NATO Grant No. 198/84. One of us (HWJB) wishes to thank M. P. Nightingale for the hospitality extended to him at the University of Rhode Island where a portion of this work was carried out.

References

1. F. Y. Wu, X. N. Wu and H. W. J. Blöte, *Phys. Rev. Lett.* **62** (1989) 2773.
2. For a review of finite-size analysis, see M. P. Nightingale, *J. Appl. Phys.* **53** (1982) 7927; and M. N. Barber in *Phase Transitions and Critical Phenomena*, eds. C. Domb and J. L. Lebowitz, (Academic Press, 1983), Vol. 8.
3. M. P. Nightingale, *Proc. Kon. Ned. Ak. Wet.* **B82** (1979) 235; M. P. Nightingale, *Phys. Lett.* **59A** (1975) 486.
4. H. W. J. Blöte and M. P. M. den Nijs, *Phys. Rev.* **B37** (1988) 1766.
5. T. D. Schultz, D. C. Mattis and E. H. Lieb, *Rev. Mod. Phys.* **36** (1964) 856.
6. V. Privman and M. E. Fisher, *Phys. Rev.* **B30** (1984) 322.
7. M. P. Nightingale and H. W. J. Blöte, *J. Phys.* **A16** (1983) L657.
8. J. Cardy, *J. Phys.* **A17** (1984) L385.
9. M. E. Fisher, *Proc. Enrico Fermi Int. School of Physics*, ed. M.S. Green, (Academic Press, 1971).
10. B. Derrida and J. Vannimenus, *Colloque sur les Méthodes de Calcul pour l'Etude de Phénomènes Critiques de Carry le Rouet*, (Springer, 1980).
11. T. D. Lee and C. N. Yang, *Phys. Rev.* **87** (1952) 410.
12. W. W. Bradbury and R. Fletcher, *Num. Math.* **9** (1969) 259; see also e.g. W. H. Press, B. P. Flannery, S. A. Teukolsky, and W. T. Vetterling, *Numerical Recipes*, (Cambridge University Press, 1986).
13. H. W. J. Blöte and M. P. Nightingale, *Physica* **112A** (1982) 405.